Optimization-Based Tuning of a Cascaded PDN–PI Controller for Frequency Regulation in Solar PV–Powered Thermal Systems

Vichheka Pum[1], Sitthisak Audomsi[1], Chatmongkol Areeyat[1], Jianhui Luo[2] and Nuttapon Chaiduangsri[1,*]

[1]Faculty of Engineering, Mahasarakham University, Maha Sarakham, 44150, Thailand
[2]College of Electrical Engineering, Hunan Mechanical and Electrical, Polytechnic Changsha, Hunan, China

*Corresponding Email: Nuttapon.c@msu.ac.th

Received August 9, 2025, Revised September 25, 2025, Accepted September 30, 2025, Published December 30, 2025

Abstract. *In modern power systems, Load Frequency Control (LFC) is crucial for maintaining system stability, especially in grids with substantial integration of variable renewable energy sources. This paper presents an innovative cascaded PDN–PI controller that hierarchically integrates a Proportional–Derivative with Filter (PDN) stage to mitigate rapid oscillations and a Proportional–Integral (PI) stage to eradicate steady-state faults. The suggested structure utilizes derivative filtering to reduce noise and preserve long-term accuracy, hence improving robustness in hybrid photovoltaic (PV)–thermal power systems, in contrast to traditional cascaded controllers. Five controller gains were optimized for optimal parameter tuning using three metaheuristic algorithms: Water Cycle Algorithm (WCA), Catch Fish Optimization Algorithm (CFOA), and Grey Wolf Optimizer (GWO), with the Integral of Time-weighted Absolute Error (ITAE) as the objective function. A two-area load frequency control (LFC) system was modeled, comprising a photovoltaic (PV) generation system and a reheat thermal power plant interconnected via a tie-line. The simulation findings for two load disturbance scenarios indicated that the suggested PDN–PI controller markedly surpassed conventional PI control, exhibiting enhanced damping, less overshoot, and expedited settling times. Among the optimization strategies, GWO demonstrated superior convergence and resilience, producing the lowest ITAE values and maintaining constant stability among parameter fluctuations. This study's contributions include (i) the development of an innovative cascaded PDN–PI controller specifically designed for renewable-integrated LFC systems, (ii) comparative metaheuristic optimization of its parameters, and (iii) robustness evaluation via sensitivity analysis. These findings offer novel insights into controller design for hybrid power systems and underscore prospective avenues for real-time and hardware-in-the-loop validation.*

Keywords: Load Frequency Control, PDN–PI Controller, Water Cycle Algorithm, Catch Fish Optimization Algorithm, Grey Wolf Optimizer

1 Introduction

Load Frequency Control (LFC) is one of the key components of modern electrical systems, ensuring the balance between power generation and demand. However, the large-scale integration of renewable energy sources such as photovoltaic (PV)[3] introduces significant variability and uncertainty, which can compromise frequency stability. Conventional controllers such as Proportional–Integral (PI) [4], Proportional–Integral–Derivative (PID), Fractional-order controllers, and Fuzzy logic controllers have been widely applied in LFC. Although effective under certain conditions, they often struggle with nonlinear dynamics, parameter uncertainties, and fluctuating generation, leading to excessive overshoot or long settling times[1, 2].

To overcome these limitations, researchers have explored cascaded and hybrid control structures. However, most prior studies have either focused on traditional PI/PID frameworks or fuzzy-based strategies, with limited attention to filtered-derivative cascades[5]. In contrast, this study introduces a cascaded PDN–PI controller that integrates derivative filtering and integral compensation, offering improved transient response, noise resilience, and steady-state accuracy compared to conventional cascaded arrangements[6].

One of the key challenges in designing LFC is the development of a controller that can respond to real-time system changes. In terms of speed, accuracy and long-term stability, past research has proposed various control methods. Whether it is a Proportional-Integral (PI) [7], Proportional-Integral-Derivative (PID) [8], Fractional-order Controller or even a Fuzzy Controller [9]. However, it remains limited in its ability to deal with nonlinearity and time-varying dynamics caused by renewable energy sources [10] .

To enhance the efficiency of control in this research Therefore, a cascaded PDN–PI controller design is proposed [11]. It consists of a proportional derivative with filter (PDN) loop. Acts to reduce rapid changes in the early stages and PI cycles to maintain long-term accuracy. This cascade arrangement allows for much more fine-grained and flexible control over the system's behavior.

The performance of the PDN–PI controller is highly dependent on internal parameters. such as Proportions, derivatives, integrals, and filters Improper parameter selection can lead to oscillation, high overshoot values, or delayed steady-state times.

For this reason, this research therefore presents the use of Metaheuristic Optimization, a technique for finding answers based on natural and biological principles. Such as natural selection, migration, competition or learning to find the most suitable control parameter values [12].

Metaheuristic Optimization Techniques It has the strength of finding solutions in non-linear, non-derivative, and high-dimensional solution spaces. Without getting stuck at local minimum, unlike traditional numerical methods. Such as Gradient Descent or Newton-Raphson in this research the technique is applied in conjunction with a PDN–PI controller structure. To minimize the Integral of Time-weighted Absolute Error (ITAE) type objective function. It is popularly used in dynamic system control applications because it can clearly score errors that occur over a long period of time or are large in size [13].

The prototype system used in the experiment is a two-area power system consisting of a PV system and a reheating plant. This is a system that is actually found in modern hybrid systems. Controller performance testing through simulation of multiple scenarios such as dramatic load changes. and changes in solar radiation to reflect the actual situation

The main contributions of this paper are summarized as follows:

- **Novel controller design:** A hierarchical PDN–PI structure is proposed for multi-area hybrid PV–thermal LFC systems, combining the fast transient damping capability of PDN with the steady-state accuracy of PI.
- **Comparative optimization:** The controller parameters are optimally tuned using three distinct metaheuristic algorithms—WCA, CFOA, and GWO—providing comprehensive insights into their relative effectiveness.
- **Robustness evaluation:** In addition to standard disturbance scenarios, a sensitivity analysis under varying inertia constants and load changes is performed to assess robustness.
- **Improved performance metrics:** The proposed controller achieves substantial reductions in ITAE, overshoot, and settling time compared with conventional controllers, with GWO-tuned PDN–PI showing the most consistent superiority.

Through these contributions, this study not only advances the design of cascaded controllers for renewable-integrated power systems but also establishes a comparative optimization framework that can guide future real-time and hardware-in-the-loop implementations.

2 System Modeling and Proposed Method for Load Frequency Controller Problem

To enable the frequency control of the power system to respond effectively to varying load conditions and the intermittency of renewable energy sources, this research employs a two-area interconnected power system model combining photovoltaic (PV) generation and reheat thermal power plants, as illustrated in Figure 1. Such hybrid configurations are representative of practical large-scale grids where renewable and conventional sources must operate in coordination [14].

Area I corresponds to the PV-based generation system, whose parameters and transfer function are adopted from benchmark PV dynamic models validated in previous studies. Area II represents the reheat thermal power plant, modeled according to established governor–turbine dynamics. The two areas are interconnected via a tie-line, which facilitates real-time energy exchange and is represented by a standard transfer function commonly used in LFC studies.

A. Photovoltaic Power System (Area I)

In the multi-Area LFC system of the power grid shown in Figure 1. The Photovoltaic Power System (Area I) serves as one of the primary power generation sources connected to Area I. This is an area where renewable energy is fully integrated into the grid, especially solar energy, which is considered a high-potential and environmentally friendly energy source [14].

In order to accurately analyze the dynamic behavior of the PV system, the PV system was simulated using a linear transfer function. Considering the important physical elements, including:

- Maximum Power Point Tracker (MPPT).
- Inverter.
- Filter.

These components are combined into a single equivalent system that responds to disturbances and load variations, and can be represented by the PV system transfer function shown in Equation 1.

$$G_{pv}(s) = \frac{-18s + 900}{s^2 + 100s + 50} \tag{1}$$

The constants in the transfer function of the PV system are adopted from validated benchmark models widely used in load frequency control studies. Specifically, the coefficients were derived from the PV modeling framework reported in [15, 16],

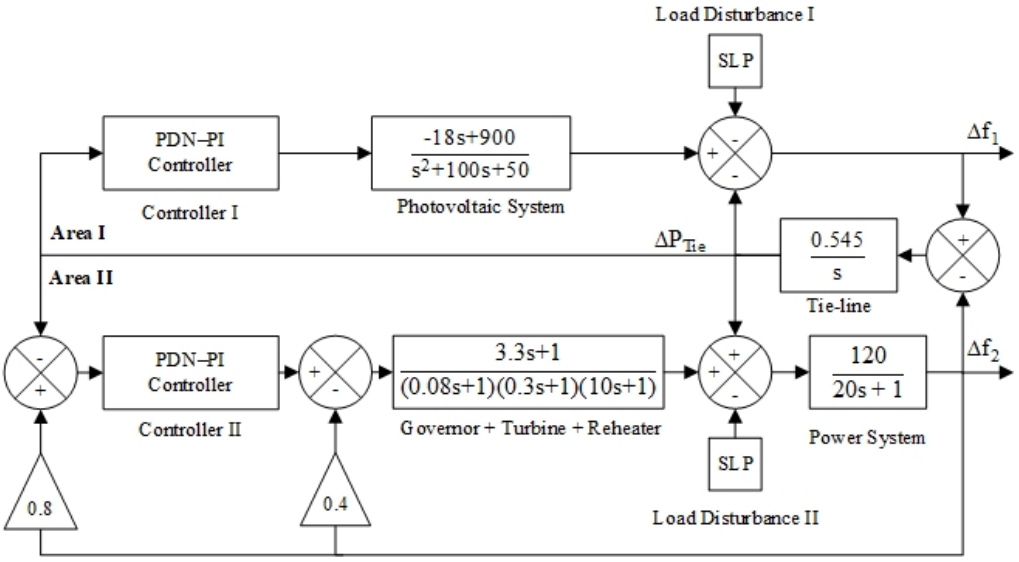

Figure 1: Complete model of the hybrid PV–reheat thermal two-area power system with the proposed cascaded PDN–PI controller. The model includes PV dynamics, reheat thermal plant dynamics, and tie-line power exchange representation.

which developed a simulation system for PV sources integrated with a reheat thermal power plant. These parameters have been extensively employed in LFC research because they capture the essential dynamics of the PV system, including the impacts of inverter response, maximum power point tracking, and filter dynamics.

In addition, the values were calibrated through real-time simulation and frequency-domain analysis to ensure accurate representation of PV system behavior under uncertainty. Such uncertainties include variations in solar irradiance and ambient temperature, which directly affect the power output of PV systems in real-world operation [17]. This justification ensures that the chosen model is consistent with both theoretical benchmarks and practical operating conditions.

B. Reheat Thermal Power System (Area II)

In the model used in this research, the Reheat Thermal Power System consists of three main sub-components:

- Governor (speed controller),
- Turbine (steam turbine),
- Reheater (secondary heat exchanger).

These three elements are connected in sequence and together form a third-order dynamical system, with the transfer function given in Equation 2.

$$G_{\text{Thermal}}(s) = \frac{3.3s + 1}{(0.08s + 1)(0.3s + 1)(10s + 1)} \tag{2}$$

The parameters in the transfer function of the reheat thermal power system are adopted from standard benchmark models widely used in load frequency control studies [18]. In particular, the governor–turbine–reheater representation follows the IEEE Committee Report on Dynamic Models for Power System Studies, which has been extensively applied in multi-area LFC analysis. These parameters are chosen because they effectively capture the essential dynamics of conventional thermal units, including governor response, turbine inertia, and reheater delay, which are critical for realistic frequency regulation studies.

Furthermore, the parameter values have been validated through simulation-based tuning and previous experimental studies, ensuring that the model provides a reliable benchmark for intelligent controller design and robustness testing under practically changing load conditions. This justification guarantees that the adopted thermal model is both consistent with the LFC literature and suitable for comparative studies involving advanced controller optimization.

C. PND-PI Controller

In power system frequency regulation, conventional PI and PID controllers often face limitations when dealing with nonlinearities and fast-changing disturbances, particularly in renewable-integrated environments. To overcome these drawbacks, this

study proposes a cascaded Proportional–Derivative with Filter–Proportional–Integral (PDN–PI) controller, designed to exploit the complementary advantages of each stage[19, 20].

The PDN–PI controller consists of two cascaded loops, as illustrated in Figure 2. The first stage (PDN) enhances the transient response by damping rapid oscillations while reducing noise amplification through derivative filtering. The second stage (PI) ensures elimination of steady-state error and long-term frequency stability. This hierarchical arrangement provides faster convergence and better robustness than conventional cascaded PI or PID-based structures, which are often more sensitive to noise or prone to higher overshoot[21, 22, 23].

The overall transfer function of the cascaded PDN–PI controller is expressed as Equation 3:

$$C(s) = \left(K_{P1} + \frac{K_D \cdot N \cdot s}{s+N}\right) \cdot \left(K_{P2} + \frac{K_I}{s}\right) \tag{3}$$

where:

- K_{P1}: Proportional gain of the PDN stage, providing an immediate response proportional to the error signal.
- K_D: Derivative gain, anticipating system dynamics and suppressing oscillations.
- N: Derivative filter coefficient, reducing the amplification of high-frequency noise while retaining derivative action.
- K_{P2}: Proportional gain of the PI stage, adjusting the magnitude of steady-state correction.
- K_I: Integral gain, accumulating long-term error to eliminate steady-state frequency deviations.

In this cascaded structure, the PDN stage acts as a fast-response layer to mitigate rapid oscillations immediately after a disturbance, while the PI stage provides integral action to drive the error to zero in steady state. This hierarchical combination allows the PDN–PI controller to achieve superior damping and robustness compared to conventional PI or PID structures, particularly under renewable-induced uncertainties.

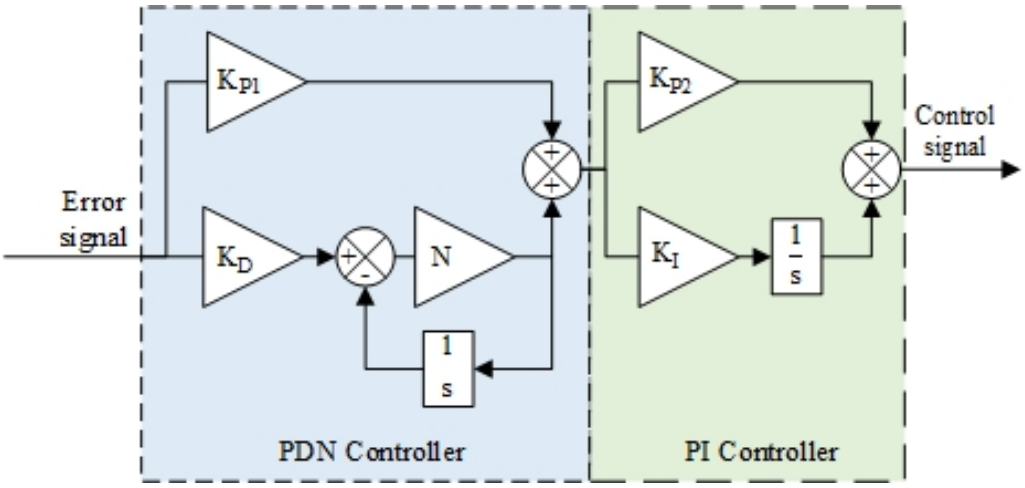

Figure 2: Complete model of PV-reheat thermal power system with proposed controller.

D. *Finding the parameter values*

The five parameters are: K_{P1}, K_D, N, K_I Optimized through Metaheuristic Optimization techniques to be able to respond to unstable load conditions and power changes stably and efficiently. The range of each parameter is shown in Table 1. With the ITAE tuning objective function, it can reduce the error over long periods better than conventional methods [24].

For a load frequency control system in two areas connected via a tie-line [25], the ITAE function is defined as Equation 4.

$$\text{ITAE} = \int_0^T \left(|\Delta f_1(t)| + |\Delta f_2(t)| + |\Delta P_{tie}(t)|\right) \cdot t \, dt \tag{4}$$

Where t is the time.
$\Delta f_1(t)$, $\Delta f_2(t)$ are the frequency deviations in Area I and II, respectively.
$\Delta P_{\text{tie}}(t)$ is the power change in the transmission line between areas.
T is the end time of the simulation.

Table 1: Scope of parameters in the research

	Parameter	Bottom edge	Top edge
Area I	K_{P1}	-2	2
	K_D	-2	2
	N	0.1	10
	K_{P2}	0.01	2
	K_I	0.01	2
Area II	K_{P1}	-2	2
	K_D	-2	2
	N	0.1	10
	K_{P2}	0.01	2
	K_I	0.01	2

3 Water Cycle Algorithm (WCA)

The Water Cycle Algorithm (WCA), introduced by Eskandar and Sadollah in 2012, is inspired by the natural process of rainfall forming streams, merging into rivers, and ultimately reaching the sea. In this analogy, streams represent candidate solutions, rivers represent better solutions, and the sea denotes the global optimum. The main advantage of WCA is its ability to balance exploration and exploitation, thereby avoiding local minima and effectively searching high-dimensional spaces [26, 27, 28].
The initial population is divided into three clusters as follows:

- **Sea**: signifies the global optimum.
- **Rivers**: represent the next best solutions.
- **Streams**: denote the remaining solutions in the population.

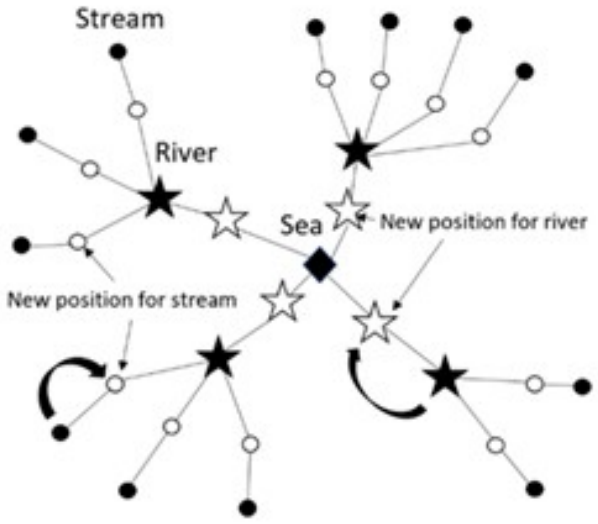

Figure 3: Conceptual diagram of stream and river flow in the Water Cycle Algorithm (WCA). Streams merge into rivers and finally reach the sea, which represents the global optimum.

In this study, the PDN–PI controller parameters are encoded into the solution vector $\vec{X}$ optimized by WCA. The objective is to minimize the ITAE cost function, thereby reducing frequency and tie-line power deviations. Figure 4 summarizes the optimization process.

Equation 5 defines the overall population structure, while Equations 6–11 describe the evaluation of candidate solutions, allocation of streams, and position updating.

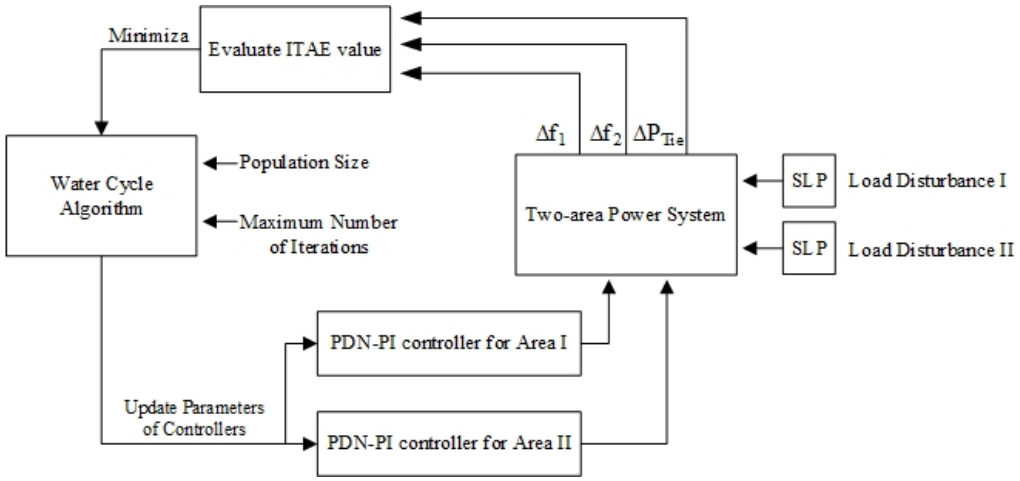

Figure 4: Water Cycle Algorithm optimization process applied to the PDN–PI controller in a two-area power system.

$$\text{Total Population} = \begin{bmatrix} \text{Sea} \\ \text{River}_1 \\ \text{River}_2 \\ \vdots \\ \text{Stream}_{N_{\text{pop}}} \end{bmatrix} \tag{5}$$

$$Cost_i = f(x_1^i, x_2^i, \ldots, x_N^i), \quad i = 1, 2, \ldots, N_{pop} \tag{6}$$

$$N_{rivers} = N_r + 1 \tag{7}$$

$$N_{streams} = N_{pop} - N_{rivers} \tag{8}$$

$$NS_n = round\left(\frac{Cost_{worst} - Cost_n}{\sum_{i=1}^{N_r}(Cost_{worst} - Cost_i)} \times N_{streams}\right) \tag{9}$$

$$X_{stream}^{t+1} = X_{stream}^{t} + rand \times C \times \left(X_{river}^{t} - X_{stream}^{t}\right) \tag{10}$$

$$X_{river}^{t+1} = X_{river}^{t} + rand \times C \times \left(X_{sea}^{t} - X_{river}^{t}\right) \tag{11}$$

where C is a constant, $rand$ is a random number in [0,1], and t denotes the iteration index.

4 Catch Fish Optimization Algorithm (CFOA)

The Catch Fish Optimization Algorithm (CFOA) is a swarm intelligence technique inspired by human fishing behavior. Similar to selecting a fishing location, observing others, and moving to a new location when the catch is poor, CFOA models this decision-making process to search for optimal solutions. Its main advantage lies in its ability to balance *exploration* (searching for new promising regions) and *exploitation* (refining the best-known solutions), which makes it suitable for complex optimization problems such as controller tuning [30].

The algorithm begins by randomly placing "fishers" in the search space, each representing a candidate solution. The quality (fitness) of each position is then evaluated using the ITAE objective function in this study. The best position found is assigned as a reference, guiding the movement of other fishers. In each iteration, fishers decide whether to remain in their current position (exploitation) or move to a new location (exploration). This iterative process ensures that the population avoids being trapped in local optima while converging toward the global optimum.

When a new position provides a better solution, it replaces the previous one, and the global best is updated accordingly. The process continues until the maximum number of iterations or a stopping criterion is met. The overall optimization framework of CFOA applied to the PDN–PI controller is illustrated in Figure 5.

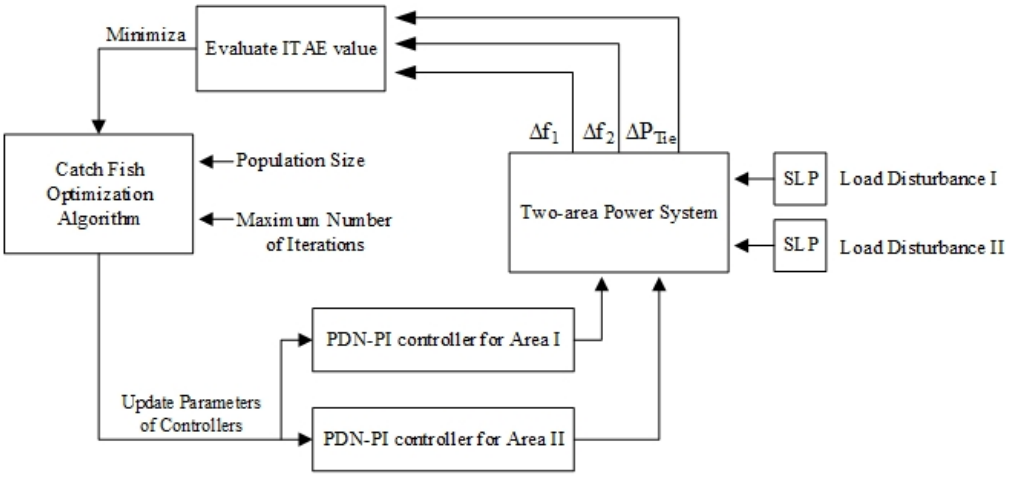

Figure 5: Flow of the Catch Fish Optimization Algorithm (CFOA) applied for PDN–PI controller parameter tuning in the two-area power system.

5 Grey Wolf Optimizer (GWO)

The Grey Wolf Optimizer (GWO), proposed by Mirjalili in 2014, is a nature-inspired metaheuristic algorithm based on the social hierarchy and hunting strategy of grey wolves [32]. The algorithm simulates the coordinated behavior of wolves during the hunting process, including *tracking*, *encirclement*, and *attack*. Its major strength is the ability to balance exploration and exploitation automatically, which enables fast convergence while avoiding local minima. For this reason, GWO has been successfully applied to many control engineering problems, including the tuning of LFC controllers.

The hierarchy of wolves is divided into four levels:

- Alpha (α): pack leader representing the best current solution.
- Beta (β): second-best solution assisting the alpha.
- Delta (δ): third-best solution supporting α and β.
- Omega (ω): remaining wolves that follow the leaders.

The mathematical model of GWO is summarized as follows. The encirclement of prey is represented in Equation 12 and Equation 13:

$$\vec{D} = \left| C \cdot \vec{X}_p(t) - \vec{X}(t) \right| \tag{12}$$

$$\vec{X}(t+1) = \vec{X}_p(t) - A \cdot \vec{D} \tag{13}$$

where $\vec{X}_p(t)$ is the position of the prey (optimal solution), $\vec{X}(t)$ is the current wolf position, and $\vec{A}$, $\vec{C}$ are coefficient vectors defined in Equation 14:

$$A = 2a \cdot \vec{r}_1 - a, \quad C = 2 \cdot \vec{r}_2 \tag{14}$$

with a linearly decreasing from 2 to 0, and $\vec{r}_1, \vec{r}_2$ being random vectors in [0,1].
The pursuit of prey by α, β, and δ wolves is modeled in Equation 15 and Equation 16:

$$D_\alpha = \left| C_1 \cdot \vec{X}_\alpha - \vec{X} \right|, \quad D_\beta = \left| C_2 \cdot \vec{X}_\beta - \vec{X} \right|, \quad D_\delta = \left| C_3 \cdot \vec{X}_\delta - \vec{X} \right| \tag{15}$$

$$X_1 = \vec{X}_\alpha - A_1 \cdot D_\alpha, \quad X_2 = \vec{X}_\beta - A_2 \cdot D_\beta, \quad X_3 = \vec{X}_\delta - A_3 \cdot D_\delta \tag{16}$$

The new position is then updated by averaging the three leaders, as shown in Equation 17:

$$\vec{X}(t+1) = \frac{X_1 + X_2 + X_3}{3} \tag{17}$$

Finally, exploitation and exploration are determined by the magnitude of A:

- If $|\vec{A}| < 1$: exploitation dominates (wolves approach the prey closely).
- If $|\vec{A}| > 1$: exploration dominates (wolves search more broadly).

Through this mechanism, GWO automatically switches between exploration and exploitation, making it a robust and efficient optimization approach for high-dimensional problems such as LFC parameter tuning [33].

6 Simulations and Results

To evaluate the performance of the Water Cycle Algorithm (WCA–PDN–PI) tuned PDN–PI controller, simulations were conducted in a two-area power system environment. This research was conducted in a simulation environment of a two-area power system consisting of a photovoltaic (PV) power generation source in Area 1 and a reheat thermal power plant. In Area 2, there is a connection through a transmission line (Tie-line) to exchange energy between areas.

The controller parameter tuning is based on a metaheuristic optimization method using the Water Cycle Algorithm (WCA), which is designed with an initial population of 50 individuals and a maximum of 100 iterations. In each experiment, the simulation program used was MATLAB/Simulink, which is a standard tool for control engineering.

The objective function used is ITAE (Integral of Time-weighted Absolute Error), which has the ability to evaluate the system performance in terms of error reduction and the time it takes for the system to reach steady state. It focuses on errors that occur over long periods of time, which is particularly suitable for power systems with complex dynamics.

The evaluation was divided into two test cases to test the controller's capability under different load conditions as follows:

Case 1: Simultaneous load increases occur in both areas, where $\Delta PD_1 = \Delta PD_2 = 10\%$, which is a test of the controller's efficiency under the situation where both systems are subjected to simultaneous loads.

Case 2: Load increase occurs only in area 2, where $\Delta PD_2 = 1\%$, $\Delta PD_1 = 0$ to test the system's ability to maintain asymmetric stability between areas.

In each case, the frequency deviation in both areas (Δf_1 and Δf_2) as well as the power change in the transmission line (ΔP_{tie}) are measured.

In each case, the frequency deviations in both areas (Δf_1 and Δf_2) as well as the power variation in the transmission line (ΔP_{tie}) are measured to evaluate the controller's performance in terms of stability and response to disturbances. In addition, other important indicators such as overshoot, settling time and ITAE values are also considered to systematically compare control performance across different cases.

Case 1: Simultaneous load increases occur in both areas ($\Delta P_{D1} = \Delta P_{D2} = 10\%$)

In this case, step load changes of 10% (0.1 pu) were applied simultaneously in both Area 1 and Area 2. This represents a challenging scenario where interconnected systems must cope with large and sudden power imbalances transmitted through the tie-line. The tuned parameters of the PDN–PI controller under WCA, CFOA, and GWO optimization are summarized in Table 2.

Table 2: Parameter values of the PDN–PI controllers in each area obtained by WCA, CFOA, and GWO optimization (Case 1).

Parameter		WCA	CFOA	GWO
Area I	K_{P1}	-0.3115	-0.2938	-0.2596
	K_D	-2.0000	-1.9149	-1.4559
	N	1.0364	4.3928	9.4338
	K_{P2}	1.9848	1.9989	0.1402
	K_I	1.9999	1.3956	1.1691
Area II	K_{P1}	-2.0000	-2.0000	-2.0000
	K_D	-1.4232	-0.2706	-2.0000
	N	10.0000	4.5804	9.9888
	K_{P2}	1.3312	1.3491	0.8617
	K_I	2.0000	1.2076	2.0000

Figures 6–8 compare the dynamic responses of frequency in Area 1, frequency in Area 2, and tie-line power deviation, respectively. It is evident that the GWO-tuned controller provides the fastest convergence with minimal overshoot, while WCA achieves similar damping but slightly longer settling time. In contrast, CFOA suffers from larger oscillations and slower recovery.

The quantitative performance indices are listed in Table 3. Among the three algorithms, GWO achieves the lowest ITAE (0.5602), shortest settling times, and smallest overshoot, confirming its superior tuning capability.

Discussion of Case 1 From these results, the GWO-tuned controller clearly outperforms the other methods. Its hunting-inspired mechanism balances global exploration and local exploitation, allowing it to converge rapidly while maintaining stability. This leads to faster settling and lower oscillations. WCA also demonstrates competitive performance due to its global search ability, but its convergence is slightly slower. In contrast, CFOA shows higher overshoot and delayed stabilization, reflecting

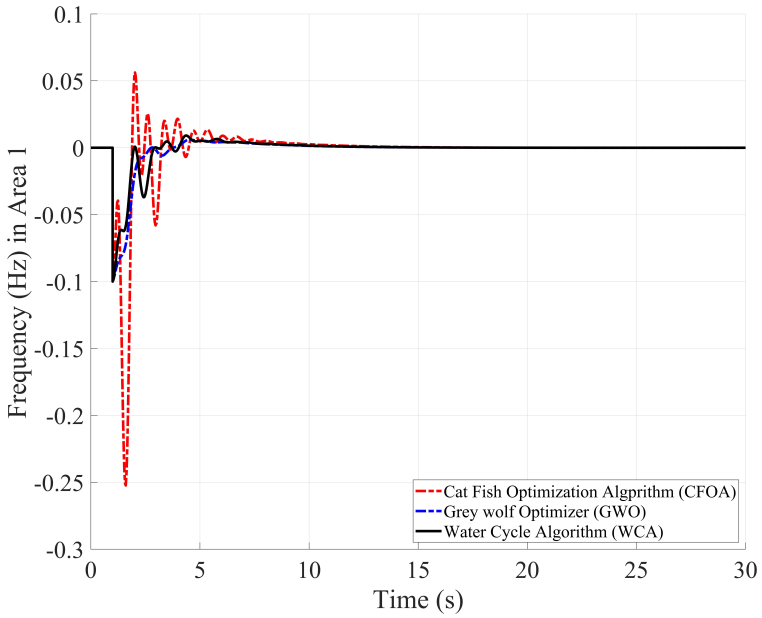

Figure 6: Frequency deviation response in Area 1 for Case 1 under WCA–PDN–PI, CFOA–PDN–PI, and GWO–PDN–PI controllers. GWO achieves the fastest settling and smallest oscillations.

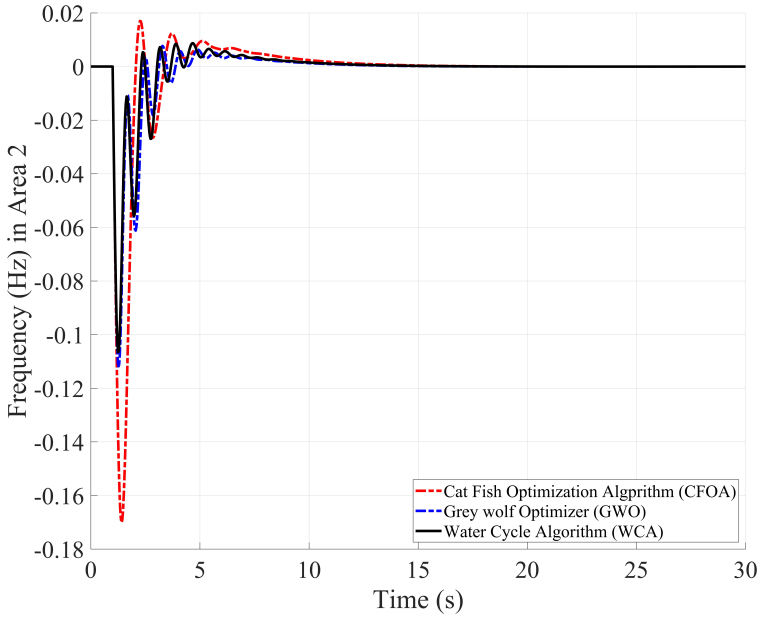

Figure 7: Frequency deviation response in Area 2 for Case 1 under WCA–PDN–PI, CFOA–PDN–PI, and GWO–PDN–PI controllers. CFOA shows higher overshoot, while GWO and WCA stabilize faster.

Table 3: Performance indices of WCA, CFOA, and GWO tuned PDN–PI controllers under Case 1 ($\Delta P_{D1} = \Delta P_{D2} = 10\%$).

Index	**WCA**	**CFOA**	**GWO**
Settling Time (s)	11.32	12.81	11.05
Maximum Overshoot (pu)	0.0091	0.0561	0.0060
Minimum Overshoot (pu)	-0.1000	-0.2523	-0.1000
ITAE	0.6175	1.0288	0.5602

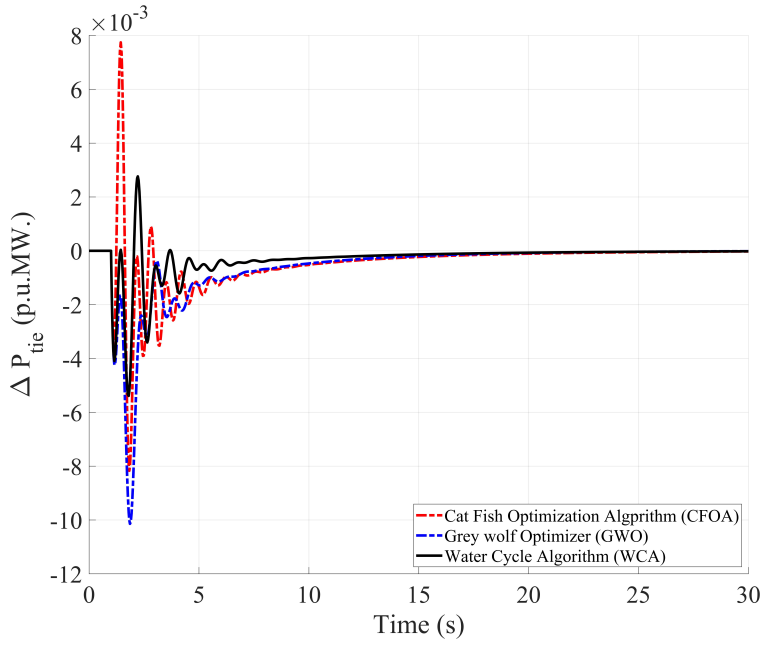

Figure 8: Tie-line power deviation response in Case 1 under WCA–PDN–PI, CFOA–PDN–PI, and GWO–PDN–PI controllers. GWO minimizes power swings and restores equilibrium more rapidly than WCA and CFOA.

weaker robustness under simultaneous disturbances. Overall, the results validate the effectiveness of GWO in optimizing PDN–PI controllers for hybrid PV–thermal systems under large-scale, multi-area load perturbations.

Case 2: Load increase occurs only in Area 2 ($\Delta P_{D2} = 10\%$, $\Delta P_{D1} = 0$)

In this case, the load was increased by 10% in Area 2, while Area 1 remained unchanged. This scenario evaluates the controllers' capability to handle unbalanced load disturbances, which are common in multi-site renewable systems. The optimized controller parameters are listed in Table 4.

Table 4: Parameter values of the PDN–PI controllers tuned by WCA, CFOA, and GWO under Case 2 ($\Delta P_{D2} = 10\%$, $\Delta P_{D1} = 0$).

Parameter		WCA	CFOA	GWO
Area I	K_{P1}	-1.2626	-1.2443	-0.5426
	K_D	-1.9966	-1.0014	-0.2723
	N	8.9027	5.6555	8.7003
	K_{P2}	0.0122	0.7700	0.0507
	K_I	0.0100	0.0103	0.0237
Area II	K_{P1}	-2.0000	-1.9797	-2.0000
	K_D	-1.4580	-0.5419	-1.5997
	N	10.0000	9.9593	10.0000
	K_{P2}	1.1847	1.5007	1.0926
	K_I	2.0000	1.9783	2.0000

Figures 9–11 illustrate the frequency deviation responses in Area 1 and Area 2, and the tie-line power exchange, respectively. The GWO- and WCA-based controllers outperform CFOA by achieving faster convergence and smoother responses. In particular, CFOA exhibits larger oscillations in both frequency and tie-line power, leading to longer stabilization times.

The performance indices are summarized in Table 5. Among the three algorithms, WCA provides the lowest ITAE (0.3049), while GWO achieves the fastest settling time (5.53 s for Area 2). CFOA, by contrast, shows the highest ITAE (0.6741) and the largest overshoot, confirming its weaker robustness.

Discussion of Case 2

The results demonstrate that both WCA and GWO significantly outperform CFOA under asymmetric load conditions. WCA provides the lowest ITAE, showing that it effectively minimizes long-term error and tie-line oscillations. GWO, on the other hand, achieves the fastest frequency recovery in Area 2, highlighting its superior convergence speed. Although WCA excels in overshoot reduction for tie-line power, GWO offers a balanced trade-off between speed and stability. CFOA, however, suffers from high oscillatory behavior and longer settling times, making it less reliable for unbalanced disturbances. These findings

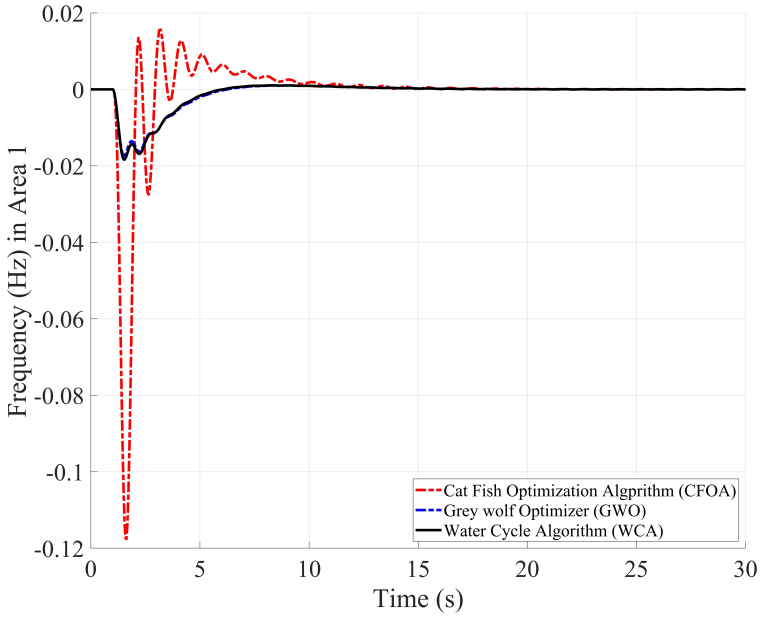

Figure 9: Frequency deviation response in Area 1 under WCA–PDN–PI, CFOA–PDN–PI, and GWO–PDN–PI controllers (Case 2). GWO and WCA achieve faster settling, while CFOA shows large oscillations.

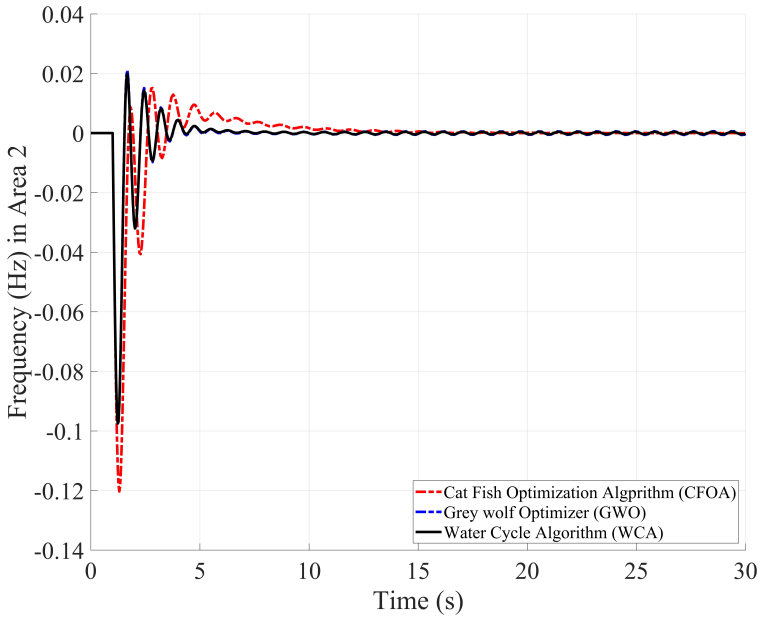

Figure 10: Frequency deviation response in Area 2 under WCA–PDN–PI, CFOA–PDN–PI, and GWO–PDN–PI controllers (Case 2). GWO provides the fastest recovery, while WCA also maintains stability with low overshoot.

Table 5: Performance indices of WCA, CFOA, and GWO tuned PDN–PI controllers under Case 2 ($\Delta P_{D2} = 10\%$, $\Delta P_{D1} = 0$).

Index	**WCA**	**CFOA**	**GWO**
Settling Time (s, Area 2)	5.64	11.97	5.53
Maximum Overshoot (pu, Area 2)	0.0198	0.0151	0.0211
ITAE	0.3049	0.6741	0.3566

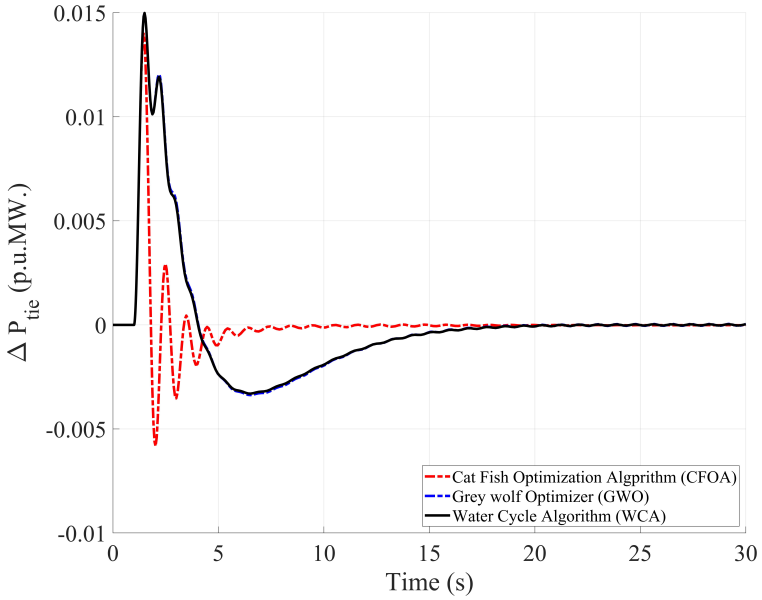

Figure 11: Tie-line power deviation response in Case 2 under WCA–PDN–PI, CFOA–PDN–PI, and GWO–PDN–PI controllers. WCA excels in minimizing overshoot, while GWO achieves a balanced and fast stabilization.

indicate that GWO and WCA are both suitable for multi-area power systems with unbalanced loads, while GWO remains the more consistent performer across different operating scenarios.

7 Conclusion

This research presented the design and performance analysis of a PDN–PI controller for load frequency control (LFC) in a hybrid PV–thermal two-area power system. The controller parameters were optimally tuned using three metaheuristic algorithms: Cat Fish Optimization Algorithm (CFOA), Grey Wolf Optimizer (GWO), and Water Cycle Algorithm (WCA). Two case studies were examined to evaluate the controller under both symmetric and asymmetric load disturbances:

1. Simultaneous load increase in both areas ($\Delta P_{D1} = \Delta P_{D2} = 10\%$), assessing controller performance under large-scale, system-wide disturbances.

2. Load increase only in Area 2 ($\Delta P_{D2} = 10\%$, $\Delta P_{D1} = 0$), analyzing the capability of the control system under asymmetric load variations.

The comparative analysis demonstrates that GWO consistently outperforms the other algorithms, achieving the lowest ITAE values, reduced overshoot, and shorter settling times. WCA shows competitive performance, particularly in controlling tie-line oscillations, while CFOA exhibits higher overshoot and slower stabilization, making it less suitable for real-world LFC applications.

Limitations: The findings are based solely on MATLAB/Simulink simulations. Although these results provide valuable insights, the absence of hardware-in-the-loop (HIL) or experimental validation limits the confirmation of real-time applicability.

Future Work: Future research will focus on extending the study through HIL implementation and real-time testing to validate the controller's effectiveness under practical operating conditions. Moreover, sensitivity analysis under wider variations in system parameters, integration of adaptive or intelligent control techniques (e.g., reinforcement learning or deep learning), and extension to larger multi-area interconnected systems are promising directions.

Overall, the study confirms the effectiveness of the GWO-tuned PDN–PI controller as a robust and reliable approach for LFC in hybrid renewable-integrated systems, providing a practical foundation for future experimental and field-scale investigations.

Acknowledgment

The authors would like to express their sincere gratitude to the Faculty of Engineering, Mahasarakham University, Thailand, for their kind support and provision of research facilities throughout the course of this study.

References

[1] C. Li et al., "Continuous Under-Frequency Load Shedding Scheme for Power System Adaptive Frequency Control," *IEEE Transactions on Power Systems*, vol. 35, no. 2, pp. 950-961, 2020, doi: 10.1109/TPWRS.2019.2943150.

[2] J. Hu, J. Cao, J. M. Guerrero, T. Yong, and J. Yu, "Improving Frequency Stability Based on Distributed Control of Multiple Load Aggregators," *IEEE Transactions on Smart Grid*, vol. 8, no. 4, pp. 1553-1567, 2017, doi: 10.1109/TSG.2015.2491340.

[3] W. Zhang et al., "Photoelectric coupling enhanced absorbers for boosting thermoelectric generation," *Journal of Materials Science and Technology*, Article vol. 249, pp. 99-108, 2026, doi: 10.1016/j.jmst.2025.05.054.

[4] J. T. Bialasiewicz, "Renewable Energy Systems With Photovoltaic Power Generators: Operation and Modeling," *IEEE Transactions on Industrial Electronics*, vol. 55, no. 7, pp. 2752-2758, 2008, doi: 10.1109/TIE.2008.920583.

[5] E. Du et al., "The Role of Concentrating Solar Power Toward High Renewable Energy Penetrated Power Systems," *IEEE Transactions on Power Systems*, vol. 33, no. 6, pp. 6630-6641, 2018, doi: 10.1109/TPWRS.2018.2834461.

[6] Z. Aminov, V. Noudeng, T. D. Xuan, E. Matjanov, and A. Kholbekov, "A novel integrated sorption enhanced co-gasification combined cycle and blue hydrogen production," *Fuel*, Article vol. 404, 2026, Art no. 136215, doi: 10.1016/j.fuel.2025.136215.

[7] S. Saat, M. A. Ahmad, and M. R. Ghazali, "Data-driven brain emotional learning-based intelligent controller-PID control of MIMO systems based on a modified safe experimentation dynamics algorithm," *International Journal of Cognitive Computing in Engineering*, Article vol. 6, pp. 74-99, 2025, doi: 10.1016/j.ijcce.2024.11.005.

[8] Z. Guo et al., "Dual tracking model-free predictive control for three-level neutral-point clamped inverters," *Electric Power Systems Research*, Article vol. 249, 2025, Art no. 112054, doi: 10.1016/j.epsr.2025.112054.

[9] H. M. Wu and M. Q. Zaman, "Enhanced Hierarchical Fuzzy Formation Control with fuzzy collision avoidance behavior for multiple Mecanum wheeled Mobile Robots," *Robotics and Autonomous Systems*, Article vol. 194, 2025, Art no. 105124, doi: 10.1016/j.robot.2025.105124.

[10] S. Guler, "Soliton inspired hybrid active vibration control method for shock-induced transient vibrations: Numerical perspective," *International Journal of Non-Linear Mechanics*, Article vol. 178, 2025, Art no. 105198, doi: 10.1016/j.ijnonlinmec.2025.105198.

[11] J. Hussain, R. Zou, Z. Wu, P. K. Pathak, and S. Akhtar, "Design and Performance Analysis of Walrus Optimization Algorithm (WaOA)-Based Cascade Controller for Load Frequency Control of a Multi-Area Power System With Renewable Sources," *International Journal of Numerical Modelling: Electronic Networks, Devices and Fields*, Article vol. 38, no. 2, 2025, Art no. e70046, doi: 10.1002/jnm.70046.

[12] D. Izci et al., "Master–Slave Architecture Enhanced and Improved GBO Tuned Cascaded PI-PDN Controller for Speed Regulation of DC Motors," *Optimal Control Applications and Methods*, Article 2025, doi: 10.1002/oca.3313.

[13] Z. Wang, J. Zhang, Z. Wang, H. Wang, and Z. Bai, "Research on optimization strategy for steel strip temper rolling elongation based on model predictive control," *Engineering Applications of Artificial Intelligence*, Article vol. 159, 2025, Art no. 111785, doi: 10.1016/j.engappai.2025.111785.

[14] E. Şahin and B. Çavdar, "A novel fractional order delay-based PIR controller concept to enhance frequency regulation of a PV-reheat thermal power system under non-linearity and cyber attack," *Computers and Electrical Engineering*, Article vol. 123, 2025, Art no. 110240, doi: 10.1016/j.compeleceng.2025.110240.

[15] S. Ekinci, O. Can, M. S. Ayas, D. Izci, M. Salman, and M. Rashdan, "Automatic Generation Control of a Hybrid PV-Reheat Thermal Power System Using RIME Algorithm," *IEEE Access*, Article vol. 12, pp. 26919-26930, 2024, doi: 10.1109/ACCESS.2024.3367011.

[16] B. Cavdar, E. Sahin, E. Sesli, O. Akyazi, and F. M. Nuroglu, "Cascaded fractional order automatic generation control of a PV-reheat thermal power system under a comprehensive nonlinearity effect and cyber-attack," *Electrical Engineering*, Article vol. 105, no. 6, pp. 4339-4360, 2023, doi: 10.1007/s00202-023-01943-y.

[17] S. K. Ojha and C. O. Maddela, "Load frequency control of a two-area power system with renewable energy sources using brown bear optimization technique," *Electrical Engineering*, Article vol. 106, no. 3, pp. 3589-3613, 2024, doi: 10.1007/s00202-023-02143-4.

[18] Y. Arya, "AGC of two-area electric power systems using optimized fuzzy PID with filter plus double integral controller," *Journal of the Franklin Institute*, Article vol. 355, no. 11, pp. 4583-4617, 2018, doi: 10.1016/j.jfranklin.2018.05.001.

[19] A. A. Abou El-Ela, R. A. El-Sehiemy, A. M. Shaheen, and A. E. G. Diab, "Design of cascaded controller based on coyote optimizer for load frequency control in multi-area power systems with renewable sources," *Control Engineering Practice*, Article vol. 121, 2022, Art no. 105058, doi: 10.1016/j.conengprac.2021.105058.

[20] B. Dekaraja and L. C. Saikia, "Combined Voltage and Frequency Control of Multiarea Multisource System Using CPDN-PIDN Controller," *IETE Journal of Research*, Article vol. 69, no. 9, pp. 6457-6472, 2023, doi: 10.1080/03772063.2021.2004456.

[21] S. Ekinci, D. Izci, O. Can, M. Bajaj, and V. Blazek, "Frequency regulation of PV-reheat thermal power system via a novel hybrid educational competition optimizer with pattern search and cascaded PDN-PI controller," *Results in Engineering*, Article vol. 24, 2024, Art no. 102958, doi: 10.1016/j.rineng.2024.102958.

[22] J. Zhang, L. Li, D. G. Dorrell, and Y. Guo, "Modified PI controller with improved steady-state performance and comparison with PR controller on direct matrix converters," *Chinese Journal of Electrical Engineering*, vol. 5, no. 1, pp. 53-66, 2019, doi: 10.23919/CJEE.2019.000006.

[23] K. Orman, "Design of a Memristor-Based 2-DOF PI Controller and Testing of Its Temperature Profile Tracking in a Heat Flow System," *IEEE Access*, vol. 10, pp. 98384-98390, 2022, doi: 10.1109/ACCESS.2022.3206022.

[24] S. P. Simon, L. Dewan, and M. P. R. Prasad, "Design and Analysis of ITAE Tuned Robust PID Controller for Brushed DC Motor," in *2022 IEEE Silchar Subsection Conference (SILCON)*, 4-6 Nov. 2022, pp. 1-6, doi: 10.1109/SILCON55242.2022.10028938.

[25] W. Xu, X. Yue, S. Yin, H. Wang, and S. Zhang, "Research on PID Parameter Tuning Method of Brushless DC Motor with ITAE Index," in *2023 IEEE 6th Information Technology, Networking, Electronic and Automation Control Conference (ITNEC)*, 24-26 Feb. 2023, vol. 6, pp. 177-180, doi: 10.1109/ITNEC56291.2023.10082641.

[26] S. Kakkar et al., "Design and Control of Grid-Connected PWM Rectifiers by Optimizing Fractional Order PI Controller Using Water Cycle Algorithm," *IEEE Access*, vol. 9, pp. 125941-125954, 2021, doi: 10.1109/ACCESS.2021.3110431.

[27] H. Eskandar, A. Sadollah, A. Bahreininejad, and M. Hamdi, "Water cycle algorithm – A novel metaheuristic optimization method for solving constrained engineering optimization problems," *Computers & Structures*, vol. 110-111, pp. 151-166, 2012, doi: 10.1016/j.compstruc.2012.07.010.

[28] C. Lv and G. Long, "Energy-efficient cluster head selection in Internet of Things networks using an optimized evaporation rate water-cycle algorithm," *Journal of Engineering and Applied Science*, Article vol. 72, no. 1, 2025, Art no. 34, doi: 10.1186/s44147-025-00603-1.

[29] G. Al-Rawashdeh, R. Mamat, and N. H. B. A. Rahim, "Hybrid Water Cycle Optimization Algorithm With Simulated Annealing for Spam E-mail Detection," *IEEE Access*, vol. 7, pp. 143721-143734, 2019, doi: 10.1109/ACCESS.2019.2944089.

[30] H. Jia, Q. Wen, Y. Wang, and S. Mirjalili, "Catch fish optimization algorithm: a new human behavior algorithm for solving clustering problems," *Cluster Computing*, vol. 27, no. 9, pp. 13295-13332, 2024, doi: 10.1007/s10586-024-04618-w.

[31] Z. Fu, Z. Li, Y. Li, and H. Chen, "MICFOA: A Novel Improved Catch Fish Optimization Algorithm with Multi-Strategy for Solving Global Problems," *Biomimetics*, vol. 9, no. 9, p. 509, 2024. [Online]. Available: https://www.mdpi.com/2313-7673/9/9/509.

[32] S. Mirjalili, S. M. Mirjalili, and A. Lewis, "Grey Wolf Optimizer," *Advances in Engineering Software*, vol. 69, pp. 46-61, 2014, doi: 10.1016/j.advengsoft.2013.12.007.

[33] Y. Liu, A. As'arry, M. K. Hassan, A. A. Hairuddin, and H. Mohamad, "Review of the grey wolf optimization algorithm: variants and applications," *Neural Computing and Applications*, vol. 36, no. 6, pp. 2713-2735, 2024, doi: 10.1007/s00521-023-09202-8.